ACS Photonics

Article

pubs.acs.org/journal/apchd5

Imaging and Steering Unidirectional Emission from Nanoantenna Array Metasurfaces

Klas Lindfors,*[,†,‡,§] Daniel Dregely,[†,‡] Markus Lippitz,[†,‡,∥] Nader Engheta,[⊥] Michael Totzeck,[#] and Harald Giessen[†]

[†]Fourth Physics Institute and Research Center SCoPE, University of Stuttgart, Pfaffenwaldring 57, 70550 Stuttgart, Germany

[‡]Max Planck Institute for Solid State Research, Heisenbergstrasse 1, 70569 Stuttgart, Germany

[§]Department of Chemistry, University of Cologne, Luxemburger Strasse 116, 50939 Cologne, Germany

[∥]Department of Physics, University of Bayreuth, Universitaetsstrasse 30, 95447 Bayreuth, Germany

[⊥]Department of Electrical and Systems Engineering, University of Pennsylvania, 200 South 33rd Street, ESE 203 Moore, Philadelphia, Pennsylvania 19104, United States

[#]Corporate Research and Technology, Carl Zeiss AG, Carl-Zeiss-Strasse 22, 73447 Oberkochen, Germany

Supporting Information

ABSTRACT: In radiofrequency antenna engineering, the array factor made long-distance communication with steerable transmission and receiving possible. At optical frequencies, low-loss signal transmission via free space by using nanoantennas is still in its infancy. Here, we suggest applying the array factor to the optical frequency regime by shaping the radiation pattern of plasmonic metasurfaces featuring nanoantenna arrays. We arrange dipolar gold nanoantennas operating at 785 nm wavelength in wavelength-sized arrays and control the phase that drives the antenna elements. We obtain collimated and unidirectional radiation from this metasurface upon illumination with circularly polarized light, which is not prone to major losses as in common plasmonic waveguide structures. We furthermore demonstrate switching the unidirectional emission to opposite directions with additional beamsteering by modifying the array factor. Our experiment corroborates the evidence for spin−orbit coupling between the helicity of light and suitably designed plasmonic metasurfaces, which can exhibit the spin-Hall effect for light.

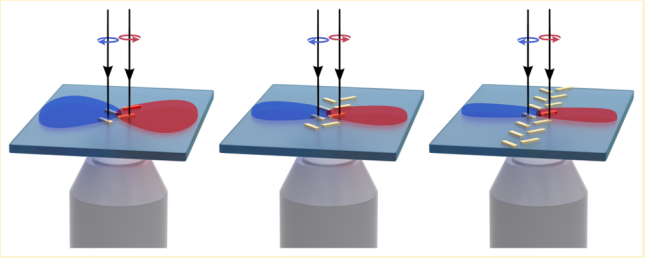

KEYWORDS: *optical nanoantenna, array factor, metasurface, luminescent imaging, beam steering*

Plasmon resonant nanoparticles enable confining incident far-field radiation to the nanoscale and they aid in generating efficient radiation from subwavelength emitters.[1] Owing to their function, plasmon resonant nanoparticles are called optical nanoantennas. They have been used in a large variety of applications such as ultrasensitive sensing,[2−5] enhancing nonlinear frequency conversion,[6−10] and modifying transition rates and emission characteristics of single-photon sources.[11−14] By arranging optical nanoantennas in arrays to form a metasurface, the spatial distribution of the amplitude, phase, and polarization of the transmitted field can be controlled.[15−18] Recent demonstrations of applications of metasurfaces include holography,[19,20] optical elements,[21−23] nonlinear frequency conversion,[24−26] and visibility cloaking.[27] One of the key application areas of optical antennas is in transmitting and receiving optical signals in order to couple free-space optical communication to nanoscale objects.[28−30] Wireless links to transmit optical power between distant optical antennas have recently been studied both theoretically[31] and experimentally,[32] demonstrating low-loss communication between nanoscale objects. Here we experimentally study the use of metasurfaces, consisting of optical nanoantenna arrays, to engineer the radiation pattern for improved wireless power transmission applications. We also emphasize an important requirement in wireless optical links, namely, highly unidirectional radiation in the direction of the receiver.

The far-field radiation pattern of an optical antenna is one of the key properties of the device. It characterizes the ability of the device to transfer localized energy to a desired direction in the far-field. Owing to reciprocity, this is equivalent to the ability of an antenna to receive energy from a distant source at a given direction. When only the lowest order plasmon resonance occurs, an optical antenna can be viewed as an electric point dipole (Figure 1a). In this case, the far-field properties of the structure are completely determined by the orientation and magnitude of the dipole moment. As in their radio frequency (rf) counterparts, by arranging dipolar nanoantennas on a metasurface in an array the far-field radiation pattern can be

Received: November 10, 2015
Published: January 20, 2016

DOI: 10.1021/acsphotonics.5b00646
ACS Photonics 2016, 3, 286−292

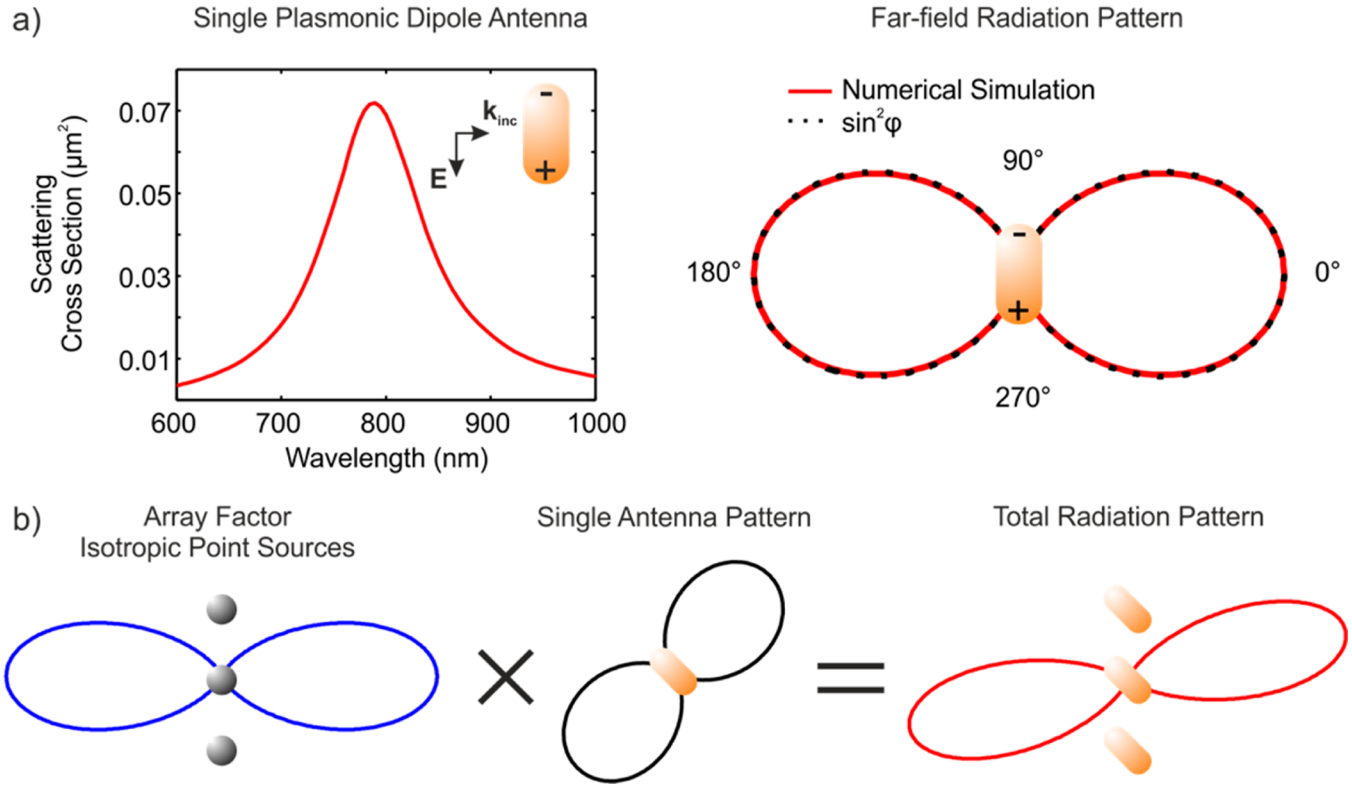

Figure 1. As in the rf scenarios, the array factor provides a flexible method to engineer light emission and reception of optical nanoantenna arrays. (a) A single gold nanorod (length 100 nm, width 50 nm, thickness 40 nm) exhibits a longitudinal plasmon resonance in the scattering spectrum (left). The calculated far-field radiation pattern at resonance is well described by a sinusoidal dipolar pattern (right). (b) When nanoantennas are arranged in an array, the radiation pattern of the nanoantenna array can be described with the help of the array factor. The total radiation pattern is simply the product of the array factor and the single antenna pattern.

engineered using the geometrical parameters of the array. A very powerful way to describe the far-field properties of the nanoantenna array is using the well-known concept of array factor.[33] The array factor fully summarizes the properties of the array, allowing separation of the properties of the array and the single antenna. Similarly to X-ray diffraction in crystals, where the diffraction pattern in the far field can be computed by the product of the structure factor and the form factor, the radiation pattern of the nanoantenna array, which is formed by a collection of identical individual radiating elements, is simply given as the product of the array factor and the radiation pattern of the isolated antenna element (Figure 1b). By controlling the phase of the signal that drives the array elements one can achieve beam steering. This functionality can be efficiently described using the array factor.[33]

We study the use of nanoantenna metasurfaces to engineer their far-field radiation pattern. We place gold nanorods on metasurfaces in linear arrays and in a fishbone shaped arrangement and map the radiation pattern using photoluminescence imaging. The devices are excited from the far-field with a tightly focused near-infrared beam with wavelength λ = 785 nm. We observe the intensity pattern around the array on the metasurface using a layer of embedded dye molecules. We first use linear arrays of antennas to achieve highly directional radiation. Then, by placing the nanoantennas in a fishbone pattern we engineer the array factor to enable unidirectional radiation with additional switching capability between two opposite directions. Finally, by controlling the phase of the signals that drive the elements in an array we manage to steer the transmitted radiation continuously. All of our experimental observations are in excellent agreement with a theoretical model treating the nanoantennas as electric point dipoles.

We fabricate metasurfaces that consist of arrays of rod-shaped plasmonic nanoantennas on a microscope cover glass (refractive index 1.52) using electron beam lithography. We first spin-coat double layer PMMA resist with a total thickness of 200 nm on the substrate. The bottom layer (molecular weight 250000) is more sensitive than the top layer (molecular weight 950000), resulting in an undercut that facilitates lift-off processing. A 30 nm thick layer of conductive polymer (eSpacer 300Z) is spin coated on top of the resist to prevent charging of the sample. The resist is exposed and developed, and a 2 nm chromium adhesion layer and 40 nm gold are deposited on the sample using thermal evaporation. Finally, the metal is removed from the unexposed areas in a lift-off process.

To image the intensity distribution around the nanoantenna array we spin coat a 60 nm thick layer of PMMA into which we have blended IR140 dye molecules.[32,34] We cover the sample with index matching oil that has the same refractive index as the substrate. The PMMA layer has a refractive index of 1.48, thus preventing waveguiding effects. Because the metasurface with the nanoantenna array is in a homogeneous environment, perturbation of the radiation pattern, such as deflection of the radiation pattern toward the substrate, is eliminated. The nanostructures are illuminated with a tightly focused laser beam with 785 nm wavelength, which coincides with the absorption maximum of IR140. The dye molecules are excited in the optical field around the nanoantenna, resulting in fluorescence (emission maximum 850 nm) that we image in a fluorescence

DOI: 10.1021/acsphotonics.5b00646
ACS Photonics 2016, 3, 286−292

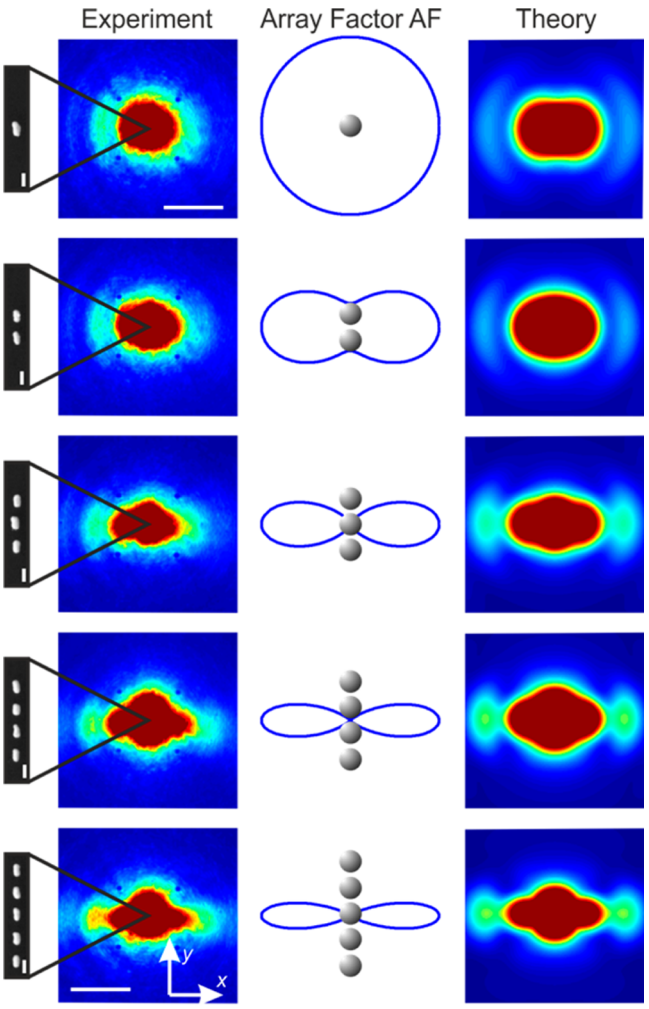

Figure 2. Directional radiation can be obtained by arranging dipolar sources in a linear array. The radiation pattern around a single nanoantenna array is visualized using a thin film of fluorescent molecules (first column from left). The radiation pattern becomes more directional as the number of elements in the array is increased. The increase in directionality is due to the change of the array factor from isotropic to directional (second column). The experimental data is in excellent agreement with calculated fluorescence patterns (third column). The scale bar for the fluorescence images is 10 μm. The scale bar for the scanning electron micrographs is 100 nm.

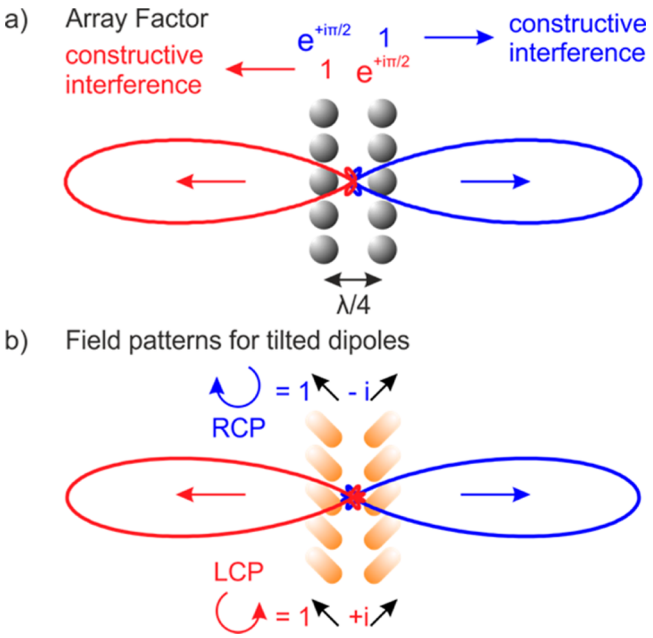

Figure 3. Two columns of nanoantennas can be used to obtain unidirectional radiation. (a) The antenna elements in the two columns oscillate 90° out of phase. When the separation between the columns is a quarter wavelength, the array factor is directed to the left or right depending on the sign of the phase difference between the antenna elements. (b) This concept can be realized using rod-shaped nanoantennas by placing them oriented at right angles to each other. Incident circularly polarized light resonant to the fundamental longitudinal plasmon results in radiation to the left/right for left/right circularly polarized incident light.

microscope. The fluorescence image reflects the intensity distribution around the nanostructure in the plane of the substrate. Full details of the experimental setup are given in the Supporting Information.

We first demonstrate the use of the array factor to increase the directionality of the radiation pattern of a linear nanoantenna array. The leftmost column of Figure 2 shows the measured fluorescence pattern around linear arrays of nanoantennas with 1−5 elements in the array. The nanostructure is in the center of each image. Here the array is illuminated with light polarized along the length of the rod along the *y*-direction. The lengths and widths of the antennas were determined from scanning electron micrographs (see Figure 2) to be 100 and 50 nm, respectively, and the period of the elements in the array is 170 nm. For these dimensions the fundamental longitudinal plasmon resonance occurs at the used 785 nm excitation wavelength. The nanoantenna thus acts as a dipolar scatterer (see Figure 1a). The fluorescence pattern is elongated in the *x*-direction for all structures, and the effect is enhanced as the number of elements in the array is increased. This is due to the change in the array factor from a fully isotropic to a highly directional function[33] (see the second column of Figure 2). The round spot in the middle of the fluorescence images originates from molecules excited directly by the incident focused beam and is not related to the nanoantenna array. When the polarization of the incident light is along the transverse direction of the nanoantennas only this background spot is observed (not depicted here).

We model the nanoantennas as electric point dipoles oriented in the *y*-direction. We first calculate the radiated electromagnetic field and use it to obtain the fluorescence pattern in the plane of the substrate taking into account the bleaching and saturation of the dye molecules. Full details about the model are given in the Supporting Information. The agreement between the measured and calculated fluorescence images is excellent (left- and right-most columns in Figure 2). In the middle column of Figure 2, we plot the array factor for the linear arrays studied here. Due to constructive interference between the elementary waves radiated by each "point" source the radiation pattern changes to be more directional when the number of elements is increased. The radiation pattern of the antenna array is simply given by the product of the array factor and the dipolar $[\sin(\varphi)^2]$ intensity distribution of the elements of the array. This illustrates how the array factor simplifies engineering of the radiation pattern. By making use of more advanced antennas with different antenna emission/receiving patterns, more complex radiation patterns can be easily engineered and realized using this concept.

DOI: 10.1021/acsphotonics.5b00646
ACS Photonics 2016, 3, 286−292

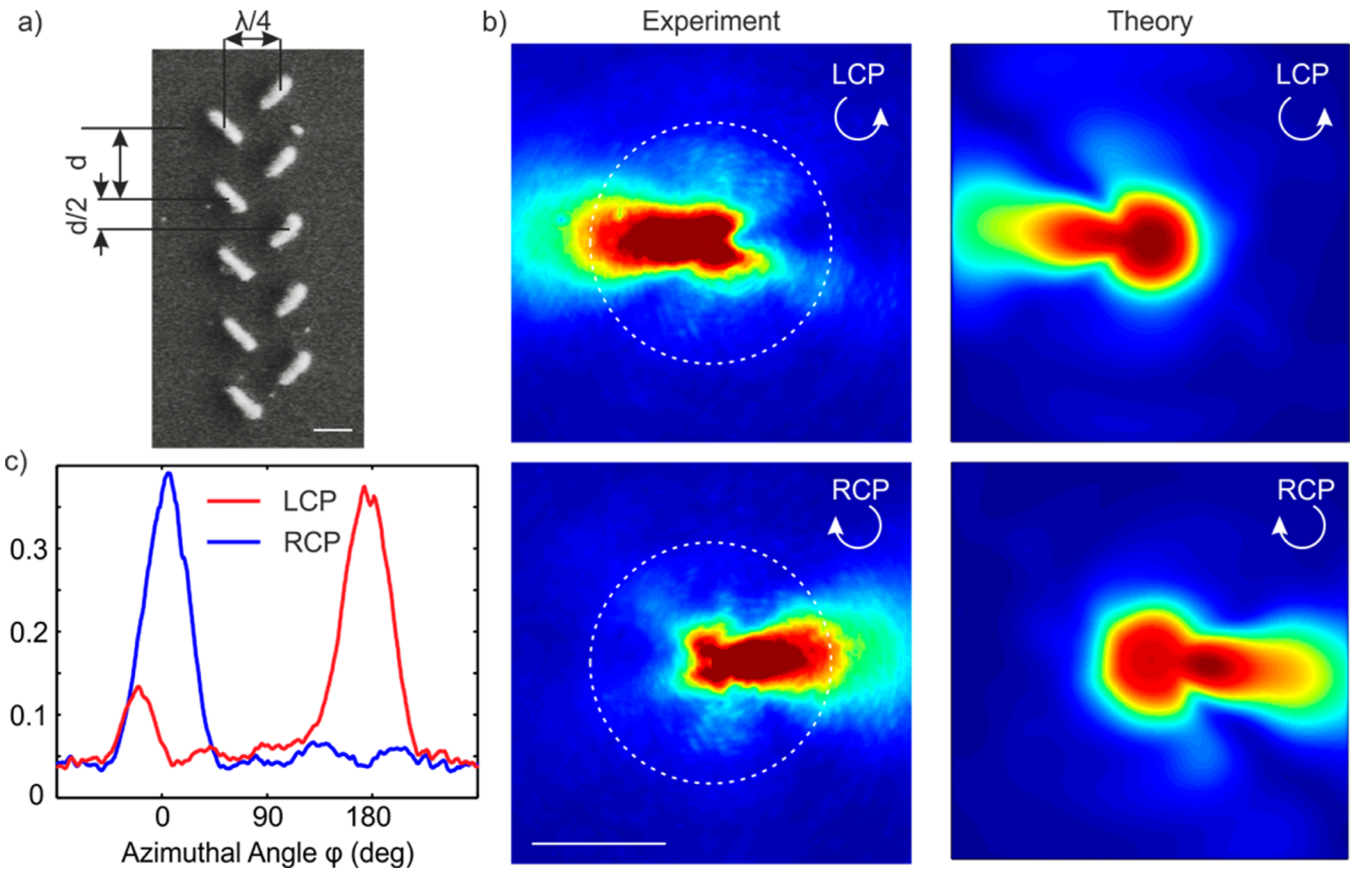

Figure 4. (a) Nanoantenna array consisting of two columns of rod-shaped nanoantennas oriented at right angles to each other results in a unidirectional radiation. The period d is 170 nm. The scale bar is 100 nm. (b) Illuminating the structure with circularly polarized light results in a unidirectional emission whose direction can be switched via the handedness of the incident light, as discussed in the main text. The scale bar is 10 μm. (c) The luminescence signal along the circular paths around the nanoantenna array shown in (b) exhibits narrow peaks in the 0 or 180° direction, depending on the handedness of the incident light.

We next use the array factor to realize unidirectional emission from a metasurface, consisting of a linear array of slanted nanoantennas. The array factor required to realize unidirectional emission is depicted in Figure 3a. The structure consists of two columns of 45° oriented nanoantennas. The columns are separated by a quarter wavelength and the elements in the two columns oscillate 90° out of phase. The phase difference in the complex electric field transmitted by the two columns can be described by a phase factor $\exp(\pm i\pi/2)$, where the sign determines, which column is ahead in phase. Propagation results in an additional phase difference between the waves emitted by the two columns described by a phase factor $\exp(\pm i\pi/2)$, where the upper(lower) sign corresponds to propagation to right(left). The total phase difference is given by the product of the two factors. We observe that the emitted waves will interfere constructively in one direction and destructively in the opposite direction as illustrated in Figure 3a.[33,35] By changing the sign of the phase difference between the antennas in the two columns, the direction of the emitted radiation can be reversed. This concept can be realized using rod-shaped nanoantennas by arranging them in two columns oriented at right angles with respect to each other (see Figure 3b). When this metasurface is illuminated with circularly polarized light resonant to the fundamental longitudinal plasmon of the antennas, the necessary phase difference between the two columns is achieved. Depending on the handedness of the incident field, the radiation is directed either to the left or to the right in the geometry displayed in Figure 3b, and switching of unidirectional radiation is achieved. We remark that, although the tilted nanorods have vertical and horizontal components of the dipole moments, the vertical components of the dipoles contribute significantly more to the radiation pattern than the horizontal ones due to the highly directional array factor. This justifies treating the array elements as "identical" antennas. Finally, we note that a similar arrangement of apertures in a gold film was recently used to achieve directional excitation of surface-plasmon polaritons, whose propagation was confined to a metal surface.[35]

The metasurface with the nanoantenna array shown in Figure 4a is used to demonstrate switchable unidirectional emission of free-space propagating radiation. We fabricate arrays of rod-shaped nanoantennas with 100 nm length, 50 nm width, and 40 nm thickness. The antennas are positioned in a similar arrangement as the one shown in Figure 3b. The separation between the two columns of antennas is 130 nm, which is equal to a quarter wavelength in the medium surrounding the nanoantennas for the light used in the experiments (free-space wavelength, 785 nm). When the array is illuminated with circularly polarized light we observe unidirectional radiation as shown in Figure 4b. The nanoantenna array is in the middle of each fluorescence image. Changing the handedness of the excitation light reverses the direction of the radiation as discussed above. When the structure is illuminated with linearly polarized light, the radiation is directed in both directions (not

DOI: 10.1021/acsphotonics.5b00646
ACS Photonics 2016, 3, 286−292

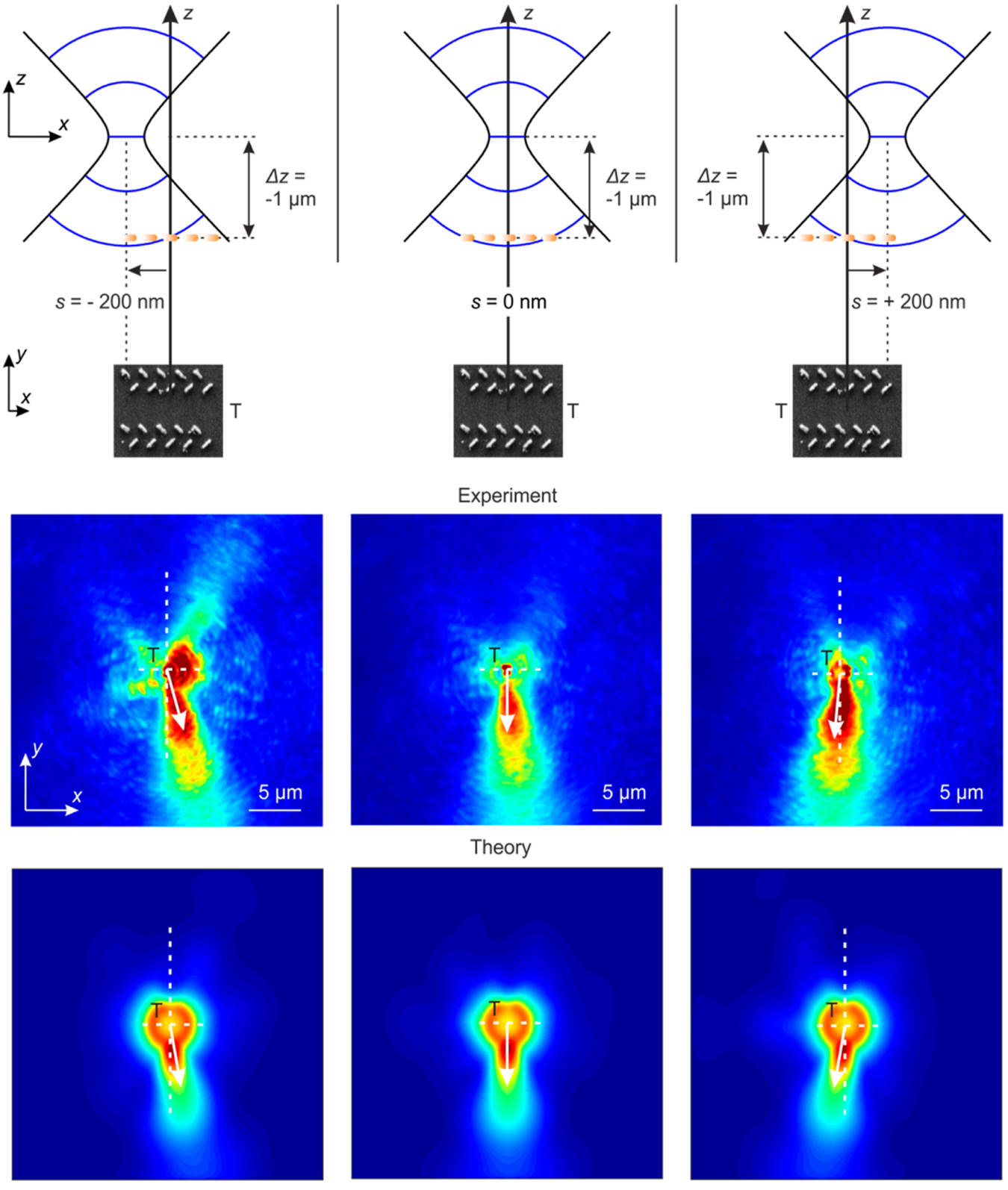

Figure 5. We control the phase of the signal driving the elements in the nanoantenna array by defocusing the tightly focused incident beam from the structure (top row). The wavefronts in the top row correspond to λ spacing. Displacing the incident beam from the center of the structure results in a phase gradient across the nanoantenna array. The SEM images of the transmitter *T* are to scale with the calculated wavefronts. When the incident beam is displaced in the *x*-direction we observe beam steering of the transmitted radiation in the fluorescence images (middle row). The direction of the beam steering can be controlled by the direction of the displacement. The experimental data are in excellent agreement with calculated fluorescence images (bottom row).

shown). We calculate the fluorescence pattern using the model introduced above, treating the antenna elements as electric point dipoles. The calculated images shown in Figure 4b are in excellent agreement with the experimental data. A small

DOI: 10.1021/acsphotonics.5b00646
ACS Photonics 2016, 3, 286−292

difference between the propagation directions of the measured and calculated radiation patterns is observed. This is due to a small offset of the position of the exciting tightly focused beam from the center of the array. We have confirmed with our theoretical model that the position of the excitation beam affects the radiation pattern.

Figure 4c shows the fluorescence signal around the nanoantenna array along a circular path of 9 μm radius around the nanostructure. We observe narrow peaks in the 0 and 180° azimuthal directions for the two different circular polarization illuminations. The observed high directionality of the emission is due to the constructive interference of the waves radiated by the antenna elements in a narrow angular range. The directionality could be further boosted by either increasing the number of elements in the array or by using more directional antennas.[28,36]

We now demonstrate continuous beam steering by controlling the phase of the exciting light impinging onto the elements in the nanoantenna array. This possibility is a key advantage of antenna arrays when transmitting optical signals. To achieve the required phase control we make use of the tightly focused beam that is incident on the sample. The wavefronts of the incident beam are strongly curved upon slight defocusing of the high-NA microscope objective (see top row in Figure 5). Moving the optical nanoantenna array a z-distance of 1 μm along the optical axis away from the focal plane and displacing the incident beam laterally results in a phase gradient across the array.

To observe beam steering from a unidirectional transmitter, we use the nanoantenna array consisting of two of the fishbone-shaped metasurfaces of gold nanorods introduced in Figure 4a (see inset of Figure 5 for a SEM image of the structure). The two metasurfaces are separated by one wavelength, resulting in an increased directionality due to constructive interference. When we center the excitation beam on the device, we observe a similar unidirectional beam as for the single fishbone metasurface, as demonstrated by the fluorescence image (middle row in Figure 5). The width of the transmitted beam is in this case narrower than for the single array due to the double array configuration (compare to Figure 4).

When we displace the incident beam away from the center of the nanoantenna array in the x-direction, we observe beam steering (middle row in Figure 5). The steering angle and direction can be controlled via the position of the incident beam, which modifies the phase of the signals driving the antenna elements. In the lowest row of Figure 5 we show the calculated fluorescence images. We note that the simulated images are in excellent agreement with the experimental data validating the point dipole model of the antennas.

In conclusion, we have used the concept of array factor to engineer the radiation pattern of nanoantennas. We demonstrated collimated radiation from a subwavelength-sized linear array of rod-shaped antennas. By arranging similar nanoantennas in a fishbone pattern and using circularly polarized incident light we obtain unidirectional radiation, which furthermore can be steered by controlling the phase driving the individual elements in the array. We compare our measured radiation patterns to field distributions calculated with a model that treats the individual optical antennas as electric point dipoles and find excellent agreement between experiment and theory. The far-field radiation patterns can be obtained by multiplying the dipolar radiation pattern with the array factor. The array factor is a powerful concept from the rf domain that offers an additional degree of freedom in designing optical nanoantenna-based devices. The simplicity of calculating the array factor lends it to numerical optimization of devices using for example genetic algorithms.[37] Dynamic control of the array factor may be realized using DNA nanotechnology[38] or nanoelectromechanical devices.[39] Determining the required changes in the array factor to obtain steering of the radiation pattern is likely to be much less time-consuming than direct numerical optimization of the multi-element plasmonic nanostructure. We expect optimized nanoantenna arrays to be a central component in future optical and optoelectronic devices. Our concept is further a manifestation of spin−orbit coupling between the helicity of light and the phase gradient of plasmonic metasurfaces,[40,41] which can lead to the photonic spin-Hall effect[42,43] and broadband optical components.[44,45]

■ ASSOCIATED CONTENT

Supporting Information

The Supporting Information is available free of charge on the ACS Publications website at DOI: 10.1021/acsphotonics.5b00646.

Sample characterization and details on the theoretical model for luminescence images (PDF).

■ AUTHOR INFORMATION

Corresponding Author

*E-mail: klas.lindfors@uni-koeln.de.

Notes

The authors declare no competing financial interest.

■ ACKNOWLEDGMENTS

We would like to thank ERC (Complexplas), BMBF, DFG, Baden-Württemberg-Stiftung, and Alexander-von-Humboldt foundation for support. D.D. additionally acknowledges support by the Carl-Zeiss-Stiftung and K.L. a grant from the Academy of Finland (Project 252421). We thank D. Proepper for ellipsometry measurement of the dye film and P. V. Braun and J. Y. Chin for stimulating discussions. We additionally would like to thank J. Weis and the Nanostructuring Lab team of the Max Planck Institute for Solid State Research for help with sample fabrication and Nikolai Strohfeldt with the TOC graphic.

■ REFERENCES

(1) Novotny, L.; Van Hulst, N. Antennas for Light. *Nat. Photonics* **2011**, *5*, 83−90.

(2) Wu, C.; Khanikaev, A. B.; Adato, R.; Arju, N.; Yanik, A. A.; Altug, H.; Shvets, G. Fano-Resonant Asymmetric Metamaterials for Ultrasensitive Spectroscopy and Identification of Molecular Monolayers. *Nat. Mater.* **2011**, *11*, 69−75.

(3) Nie, S.; Emory, S. R. Probing Single Molecules and Single Nanoparticles by Surface-Enhanced Raman Scattering. *Science* **1997**, *275* (5303), 1102−1106.

(4) Zijlstra, P.; Paulo, P. M. R.; Orrit, M. Optical Detection of Single Non-Absorbing Molecules Using the Surface Plasmon Resonance of a Gold Nanorod. *Nat. Nanotechnol.* **2012**, *7*, 379−382.

(5) Ament, I.; Prasad, J.; Henkel, A.; Schmachtel, S.; Sönnichsen, C. Single Unlabeled Protein Detection on Individual Plasmonic Nanoparticles. *Nano Lett.* **2012**, *12*, 1092−1095.

(6) Klein, M. W.; Enkrich, C.; Wegener, M.; Linden, S. Second-Harmonic Generation from Magnetic Metamaterials. *Science* **2006**, *313*, 502−504.

DOI: 10.1021/acsphotonics.5b00646
ACS Photonics 2016, 3, 286−292

(7) Mühlschlegel, P.; Eisler, H.-J.; Martin, O. J. F.; Hecht, B.; Pohl, D. W. Resonant Optical Antennas. *Science* **2005**, *308*, 1607−1609.
(8) Hentschel, M.; Utikal, T.; Giessen, H.; Lippitz, M. Quantitative Modeling of the Third Harmonic Emission Spectrum of Plasmonic Nanoantennas. *Nano Lett.* **2012**, *12*, 3778−3782.
(9) Metzger, B.; Hentschel, M.; Schumacher, T.; Lippitz, M.; Ye, X.; Murray, C. B.; Knabe, B.; Buse, K.; Giessen, H. Doubling the Efficiency of Third Harmonic Generation by Positioning ITO Nanocrystals into the Hot-Spot of Plasmonic Gap-Antennas. *Nano Lett.* **2014**, *14*, 2867−2872.
(10) Aouani, H.; Rahmani, M.; Navarro-Cía, M.; Maier, S. A. Third-Harmonic-Upconversion Enhancement from a Single Semiconductor Nanoparticle Coupled to a Plasmonic Antenna. *Nat. Nanotechnol.* **2014**, *9*, 290−294.
(11) Curto, A. G.; Taminiau, T. H.; Volpe, G.; Kreuzer, M. P.; Quidant, R.; van Hulst, N. F. Multipolar Radiation of Quantum Emitters with Nanowire Optical Antennas. *Nat. Commun.* **2013**, *4*, 1750.
(12) Kühn, S.; Håkanson, U.; Rogobete, L.; Sandoghdar, V. Enhancement of Single-Molecule Fluorescence Using a Gold Nanoparticle as an Optical Nanoantenna. *Phys. Rev. Lett.* **2006**, *97*, 017402.
(13) Anger, P.; Bharadwaj, P.; Novotny, L. Enhancement and Quenching of Single-Molecule Fluorescence. *Phys. Rev. Lett.* **2006**, *96*, 3−6.
(14) Akselrod, G. M.; Argyropoulos, C.; Hoang, T. B.; Ciracì, C.; Fang, C.; Huang, J.; Smith, D. R.; Mikkelsen, M. H. Probing the Mechanisms of Large Purcell Enhancement in Plasmonic Nanoantennas. *Nat. Photonics* **2014**, *8*, 835−840.
(15) Yu, N.; Capasso, F. Flat Optics with Designer Metasurfaces. *Nat. Mater.* **2014**, *13*, 139−150.
(16) Yu, N.; Genevet, P.; Kats, M. A.; Aieta, F.; Tetienne, J.-P.; Capasso, F.; Gaburro, Z. Light Propagation with Phase Discontinuities: Generalized Laws of Reflection and Refraction. *Science* **2011**, *334*, 333−337.
(17) Kildishev, A. V.; Boltasseva, A.; Shalaev, V. M. Planar Photonics with Metasurfaces. *Science* **2013**, *339*, 1232009.
(18) Liu, L.; Zhang, X.; Kenney, M.; Su, X.; Xu, N.; Ouyang, C.; Shi, Y.; Han, J.; Zhang, W.; Zhang, S. Broadband Metasurfaces with Simultaneous Control of Phase and Amplitude. *Adv. Mater.* **2014**, *26*, 5031−5036.
(19) Zheng, G.; Mühlenbernd, H.; Kenney, M.; Li, G.; Zentgraf, T.; Zhang, S. Metasurface Holograms Reaching 80% Efficiency. *Nat. Nanotechnol.* **2015**, *10*, 308−312.
(20) Huang, L.; Chen, X.; Mühlenbernd, H.; Zhang, H.; Chen, S.; Bai, B.; Tan, Q.; Jin, G.; Cheah, K.-W.; Qiu, C.-W.; Li, J.; Zentgraf, T.; Zhang, S. Three-Dimensional Optical Holography Using a Plasmonic Metasurface. *Nat. Commun.* **2013**, *4*, 2808.
(21) Shalaev, M. I.; Sun, J.; Tsukernik, A.; Pandey, A.; Nikolskiy, K.; Litchinitser, N. M. High-Efficiency All-Dielectric Metasurfaces for Ultracompact Beam Manipulation in Transmission Mode. *Nano Lett.* **2015**, *15*, 6261−6266.
(22) Lin, D.; Fan, P.; Hasman, E.; Brongersma, M. L. Dielectric Gradient Metasurface Optical Elements. *Science* **2014**, *345*, 298−302.
(23) Aieta, F.; Kats, M. A.; Genevet, P.; Capasso, F. Applied Optics. Multiwavelength Achromatic Metasurfaces by Dispersive Phase Compensation. *Science* **2015**, *347*, 1342−1345.
(24) Li, G.; Chen, S.; Pholchai, N.; Reineke, B.; Wong, P. W. H.; Pun, E. Y. B.; Cheah, K. W.; Zentgraf, T.; Zhang, S. Continuous Control of the Nonlinearity Phase for Harmonic Generations. *Nat. Mater.* **2015**, *14*, 607−612.
(25) Segal, N.; Keren-Zur, S.; Hendler, N.; Ellenbogen, T. Controlling Light with Metamaterial-Based Nonlinear Photonic Crystals. *Nat. Photonics* **2015**, *9*, 180−184.
(26) Chen, P.-Y.; Argyropoulos, C.; D'Aguanno, G.; Alù, A. Enhanced Second-Harmonic Generation by Metasurface Nanomixer and Nanocavity. *ACS Photonics* **2015**, *2*, 1000−1006.
(27) Ni, X.; Wong, Z. J.; Mrejen, M.; Wang, Y.; Zhang, X. An Ultrathin Invisibility Skin Cloak for Visible Light. *Science* **2015**, *349*, 1310−1314.
(28) Curto, A. G.; Volpe, G.; Taminiau, T. H.; Kreuzer, M. P.; Quidant, R.; van Hulst, N. F. Unidirectional Emission of a Quantum Dot Coupled to a Nanoantenna. *Science* **2010**, *329*, 930−933.
(29) Tang, L.; Kocabas, S. E.; Latif, S.; Okyay, A. K.; Ly-Gagnon, D.-S.; Saraswat, K. C.; Miller, D. A. B. Nanometre-Scale Germanium Photodetector Enhanced by a near-Infrared Dipole Antenna. *Nat. Photonics* **2008**, *2*, 226−229.
(30) Knight, M. W.; Sobhani, H.; Nordlander, P.; Halas, N. J. Photodetection with Active Optical Antennas. *Science* **2011**, *332*, 702−704.
(31) Alù, A.; Engheta, N. Wireless at the Nanoscale: Optical Interconnects Using Matched Nanoantennas. *Phys. Rev. Lett.* **2010**, *104*, 213902.
(32) Dregely, D.; Lindfors, K.; Lippitz, M.; Engheta, N.; Totzeck, M.; Giessen, H. Imaging and Steering an Optical Wireless Nanoantenna Link. *Nat. Commun.* **2014**, *5*, 4354.
(33) Balanis, C. A. *Antenna Theory*; John Wiley & Sons, 2005.
(34) Ditlbacher, H.; Krenn, J. R.; Felidj, N.; Lamprecht, B.; Schider, G.; Salerno, M.; Leitner, A.; Aussenegg, F. R. Fluorescence Imaging of Surface Plasmon Fields. *Appl. Phys. Lett.* **2002**, *80*, 404.
(35) Lin, J.; Mueller, J. P. B.; Wang, Q.; Yuan, G.; Antoniou, N.; Yuan, X.-C.; Capasso, F. Polarization-Controlled Tunable Directional Coupling of Surface Plasmon Polaritons. *Science* **2013**, *340*, 331−334.
(36) Kosako, T.; Kadoya, Y.; Hofmann, H. F. Directional Control of Light by a Nano-Optical Yagi−Uda Antenna. *Nat. Photonics* **2010**, *4*, 312−315.
(37) Feichtner, T.; Selig, O.; Kiunke, M.; Hecht, B. Evolutionary Optimization of Optical Antennas. *Phys. Rev. Lett.* **2012**, *109*, 127701.
(38) Kuzyk, A.; Schreiber, R.; Zhang, H.; Govorov, A. O.; Liedl, T.; Liu, N. Reconfigurable 3D Plasmonic Metamolecules. *Nat. Mater.* **2014**, *13*, 862−866.
(39) Ou, J.-Y.; Plum, E.; Zhang, J.; Zheludev, N. I. An Electromechanically Reconfigurable Plasmonic Metamaterial Operating in the near-Infrared. *Nat. Nanotechnol.* **2013**, *8*, 252−255.
(40) Yin, X.; Ye, Z.; Rho, J.; Wang, Y.; Zhang, X. Photonic Spin Hall Effect at Metasurfaces. *Science* **2013**, *339*, 1405−1407.
(41) Shitrit, N.; Yulevich, I.; Maguid, E.; Ozeri, D.; Veksler, D.; Kleiner, V.; Hasman, E. Spin-Optical Metamaterial Route to Spin-Controlled Photonics. *Science* **2013**, *340*, 724−726.
(42) Bliokh, K. Y.; Gorodetski, Y.; Kleiner, V.; Hasman, E. Coriolis Effect in Optics: Unified Geometric Phase and Spin-Hall Effect. *Phys. Rev. Lett.* **2008**, *101*, 030404.
(43) Li, Y.; Liu, Y.; Ling, X.; Yi, X.; Zhou, X.; Ke, Y.; Luo, H.; Wen, S.; Fan, D. Observation of Photonic Spin Hall Effect with Phase Singularity at Dielectric Metasurfaces. *Opt. Express* **2015**, *23*, 1767−1774.
(44) Pu, M.; Zhao, Z.; Wang, Y.; Li, X.; Ma, X.; Hu, C.; Wang, C.; Huang, C.; Luo, X. Spatially and Spectrally Engineered Spin-Orbit Interaction for Achromatic Virtual Shaping. *Sci. Rep.* **2015**, *5*, 9822.
(45) Pu, M.; Li, X.; Ma, X.; Wang, Y.; Zhao, Z.; Wang, C.; Hu, C.; Gao, P.; Huang, C.; Ren, H.; Li, X.; Qin, F.; Yang, J.; Gu, M.; Hong, M.; Luo, X. Catenary Optics for Achromatic Generation of Perfect Optical Angular Momentum. *Sci. Adv.* **2015**, *1*, e1500396.

DOI: 10.1021/acsphotonics.5b00646
ACS Photonics 2016, 3, 286−292